energies

MDPI

Article

An Estimation of Hydraulic Power Take-off Unit Parameters for Wave Energy Converter Device Using Non-Evolutionary NLPQL and Evolutionary GA Approaches †

Mohd Afifi Jusoh, Mohd Zamri Ibrahim *, Muhamad Zalani Daud, Zulkifli Mohd Yusop and Aliashim Albani

Renewable Energy & Power Research Interest Group (REPRIG), Eastern Corridor Renewable Energy Special Interest Group, Faculty of Ocean Engineering Technology and Informatics, Universiti Malaysia Terengganu, Kuala Nerus 21030, Terengganu, Malaysia; mohd.afifi.jusoh@gmail.com (M.A.J.); zalani@umt.edu.my (M.Z.D.); zul_12521@yahoo.com (Z.M.Y.); a.albani@umt.edu.my (A.A.)

* Correspondence: zam@umt.edu.my; Tel.: +60-96683328

† This paper is an extended and revised article presented at the International Conference on Sustainable Energy and Green Technology 2019 (SEGT 2019) on 11–14 December 2019 in Bangkok, Thailand.

Abstract: This study is concerned with the application of two major kinds of optimisation algorithms on the hydraulic power take-off (HPTO) model for the wave energy converters (WECs). In general, the HPTO unit's performance depends on the configuration of its parameters such as hydraulic cylinder size, hydraulic accumulator capacity and pre-charge pressure and hydraulic motor displacement. Conventionally, the optimal parameters of the HPTO unit need to be manually estimated by repeating setting the parameters' values during the simulation process. However, such an estimation method can easily be exposed to human error and would subsequently result in an inaccurate selection of HPTO parameters for WECs. Therefore, an effective approach of using the non-evolutionary Non-Linear Programming by Quadratic Lagrangian (NLPQL) and evolutionary Genetic Algorithm (GA) algorithms for determining the optimal HPTO parameters was explored in the present study. A simulation–optimisation of the HPTO model was performed in the MATLAB/Simulink environment. A complete WECs model was built using Simscape Fluids toolbox in MATLAB/Simulink. The actual specifications of hydraulic components from the manufacturer were used during the simulation study. The simulation results showed that the performance of optimal HPTO units optimised by NLPQL and GA approaches have significantly improved up to 96% and 97%, respectively, in regular wave conditions. The results also showed that both optimal HPTO units were capable of generating electricity up to 62% and 77%, respectively, of their rated capacity in irregular wave circumstances.

Keywords: wave energy converter; hydraulic power take-off unit; parameter estimation; genetic algorithm; non-linear programming by quadratic Lagrangian

check for updates

Citation: Jusoh, M.A.; Ibrahim, M.Z.; Daud, M.Z.; Yusop, Z.M.; Albani, A. An Estimation of Hydraulic Power Take-off Unit Parameters for Wave Energy Converter Device Using Non-Evolutionary NLPQL and Evolutionary GA Approaches †. *Energies* **2021**, *14*, 79. https://dx.doi.org/10.3390/en14010079

Received: 2 December 2020
Accepted: 20 December 2020
Published: 25 December 2020

Publisher's Note: MDPI stays neutral with regard to jurisdictional claims in published maps and institutional affiliations.

Copyright: © 2020 by the authors. Licensee MDPI, Basel, Switzerland. This article is an open access article distributed under the terms and conditions of the Creative Commons Attribution (CC BY) license (https://creativecommons.org/licenses/by/4.0/).

1. Introduction

Ocean waves are one of the renewable energy resources that potentially can be exploited to produce usable electricity due to their excellent features of predictability, high energy density and high source availability [1,2]. Currently, numerous wave energy converters (WECs) have been designed, developed, tested and patented through a variety of harnessing techniques that are subjected to the characteristics of the target location such as shoreline, nearshore and offshore, as reported in [3–6]. In general, WECs are a combination of three main parts, such as a wave energy converter (WEC) device, power take-off (PTO) unit and control system unit. Recently, various types of PTO units have been developed for WEC devices based on different working principles, such as the air and water turbine-based, direct-electrical drive-based, direct-mechanical drive-based and hydraulic-based, as reported in [7,8]. A hydraulic PTO (HPTO) is considered to be the most effective PTO

for wave-activated-body (WAB) or point-absorber based WECs due to the outstanding features, including high-efficiency, high-controllability, well-adapted to the large power density ocean waves and low-frequency [9]. It has been reported in the literature that this type of PTO system's efficiency could be achieved up to 90% [10]. Furthermore, the HPTO unit is also easily constructed using standard hydraulic components, which are commonly used in other applications. Due to such a promising characteristic, the HPTO system finds its application in the majority of the WAB-WECs field.

Recently, many HPTO unit applications in various WECs have been published [11–17]. From the preliminary survey, most of the studies concentrated on the HPTO unit's efficiency without taking into account the optimal parameters of the HPTO model, such as hydraulic cylinder size, hydraulic accumulator capacity and pre-charge pressure and hydraulic motor displacement. The optimal configuration parameters of the HPTO unit is a crucial issue as it can affect the system's efficiency and the amount of output to be produced [13]. Only a few reports, for example, in [13–15], have considered this critical problem. However, the optimal parameters setting has been obtained by manually tuning these configuration parameters [13]. This method is usually prone to human error and easy to cause a non-optimal selection of the HPTO system's parameters. In addition, this approach also frequently involves a long-time process in order to obtain the optimal configuration parameters.

Presently, the optimisation of design parameters using a mathematical algorithm is an attractive method to estimate the accurate parameters during the design phase. It is due to the advancement of fast computing technologies that can be reliably used. A variety of studies were performed using different types of mathematical algorithms, such as non-linear programming by quadratic Lagrangian (NLPQL) and genetic algorithm (GA), Particle Swarm Optimization (PSO), Ant Colony Optimization (ACO), Tabu Search (TS), et cetera, in order to obtain the best parameters for the design model [18–23]. For example, GA has been used to optimise the parameters of state-of-charge (SOC) controllers for battery energy storage in photovoltaic device applications [21]. The authors emphasized that the GA-based optimisation method has accelerated the optimisation process of the considered design parameters and effectively improves the design model's performance. Similarly, in [22], different types of heuristic optimisation approaches were applied, including Gravitational Search Algorithm (GSA) and PSO, to conduct model optimization-based studies for improving the efficiency of developed power converter units. The authors had concluded that GSA-based optimisation provides the highest convergence speed and best fitness value compared to the other algorithms. Motivated by the studies presented in [21,22], an optimized new design of WEC with an HPTO unit is presented in this study.

From the WECs point of view, a similar optimisation approach has been implemented in optimising the performance of the WECs. From the preliminary survey, several studies of the GA applications for WECs optimisation have been done [24–28]. For example, in [24], GA has been used to obtain some WECs parameters, such as buoy radius, draft, generator damping and the optimal spatial layout of a WECs park. In [25], GA has been adopted to optimally design the shape and dimensions of a WEC and also the PTO and other subsystems parameters. The techno-economic aspects of energy productivity and WECs device cost have also been considered in the study. In [28], GA has been used to obtain the optimal HPTO parameters of WECs, such as hydraulic cylinder size, hydraulic accumulator capacity and pre-charge pressure, and hydraulic motor displacement without considering the hydrodynamic effects of the floater. Since the hydrodynamic effects of the floater are the vital factors in WECs design, the optimal HPTO obtained in the study is inapplicable for real wave application. Therefore, the HPTO optimisation with the consideration of the floater's hydrodynamic effects using two different types of algorithm, such as NLPQL and GA, were investigated in this present study. The optimisation approaches presented in this study can be a useful reference to other researchers and engineers of WECs in order to design an accurate and reliable HPTO unit for the future WECs application.

The paper is organised as follows. The technical descriptions of the considered WEC with HPTO unit and its important configuration parameters are given in Section 2. The simulation studies of the HPTO unit, which includes the simulation set-up process, optimisation process and evaluation of HPTO unit performance, are described in Section 3. Results and discussion are provided in Section 4, and finally, the Conclusions are given in Section 5.

2. Mathematical Modelling of WEC with HPTO Unit

The design of the WECs depends on the characteristics of the installed location. In the present study, the rotation-based WEC attached to the fixed body concept was considered, as illustrated in Figure 1. This WECs concept has been implemented in numerous studies for various investigation goals, for example, in [29–32]. This concept is suitable to be installed at shoreline, nearshore and offshore locations. In this concept, the WEC device consists of a single or multiple floating buoy or floater attached to the rotatable arm and connected to the fixed body directed towards the dominant wave direction, as depicted in Figure 1. The multi-design of floater can be used, which is dependent on the direction of the ocean wave, either single or multi-direction. Usually, the semisphere-shaped and boat-shaped floater have been considered for the offshore and nearshore location, as investigated in [29,30,33–35]. In this concept, the HPTO unit is utilised to convert the absorbed energy by the WEC device from the ocean wave to become usable electricity. A hydraulic actuator module of the HPTO unit is attached to the rotatable floater arm in order to absorb the mechanical energy produced by the WEC device, as presented in Figure 1. Meanwhile, the rest of the HPTO unit components are placed in the PTO house located on the top of the fixed-structure. In the present study, the model of WECs with a capacity of 0.1 kW was considered.

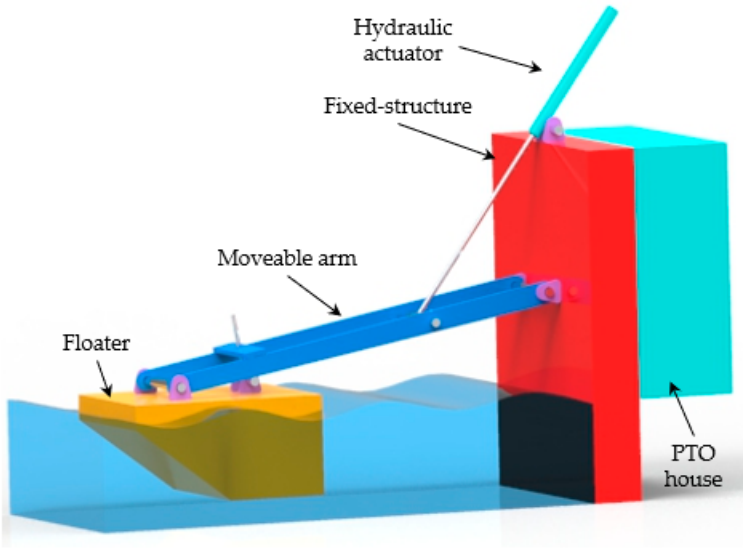

Figure 1. Conceptual design of future wave energy converter (WEC) with the hydraulic power take-off (HPTO) unit.

2.1. Hydrodynamic Motion of the Floater

In general, the hydrodynamic motion of the WEC device in real waves can be formulated in the time domain using the linear wave theory, as described in Equation (1). M_A is the D'Alembert moment of inertia, M_{ex} is the moment due to the diffracted waves, M_{rad} is the moment due to radiated waves, M_{res} is the hydrostatic restoring moment and M_{PTO} is the moment due to the HPTO unit.

$$M_A = M_{ex} - M_{rad} - M_{res} - M_{PTO} \quad (1)$$

The equation of the hydrodynamic motion in Equation (1) can be expended as given in Equation (2). Here, J_{WEC} is the inertia moment of the floater and arm. Whereas, $J_{add,\infty}$ is the added mass at the infinite frequency and $\ddot{\theta}_{arm}$ is the angular acceleration of a WEC device during the pitch motion. Then, $k_{rad}(t)$ is the radiation impulse response function, τ is the time delay and $\dot{\theta}_{arm}$ is the angular velocity of the floater's arm. Other variables such as k_{res} is the hydrostatic restoring coefficient and θ_{arm} is the angular of the floater's arm during the pitch motion. Finally, $h_{ex}(t-\tau)$ is the impulse response function of the excitation moment and η_W is the undisturbed wave elevation at the floater center point.

$$(J_{WEC} + J_{add,\infty})\ddot{\theta}_{arm}(t) + \int_0^t k_{rad}(t-\tau)\,\dot{\theta}_{arm}(t) + k_{res}\,\theta_{arm}(t) + M_{PTO}(t) \;=\; \int_{-\infty}^{\infty} h_{ex}(t-\tau)\eta_W(\tau)d\tau \tag{2}$$

The impulse response function in Equation (2) can be obtained from the hydrodynamic diffraction analysis using Computational Fluid Dynamics (CFD) software. In the present study, the hydrodynamic diffraction analysis of the WEC model was performed using ANSYS/AQWA software.

In addition, the moment due to the HPTO unit, M_{PTO} can be defined using Equations (3)–(5), where F_{PTO} is the feedback force from the HPTO unit applied to the WEC device. The variables L_1, L_2, L_3 and L_4 are the lengths between point a, b, c and d, as illustrated in Figure 2 [30,36–38]. x_p is the displacement of hydraulic cylinder piston and $L_{3,0}$ is the initial stroke of the hydraulic cylinder.

$$M_{PTO} \;=\; F_{PTO}L_4 \tag{3}$$

$$L_4 \;=\; \frac{L_1L_2sin(\theta_{arm,0}-\theta_{arm})}{L_{3,0}+x_c} \tag{4}$$

$$x_p \;=\; L_{3,0} - \sqrt{{L_1}^2 + {L_2}^2 - 2L_1L_2cos(\theta_{arm,0}-\theta_{arm})} \tag{5}$$

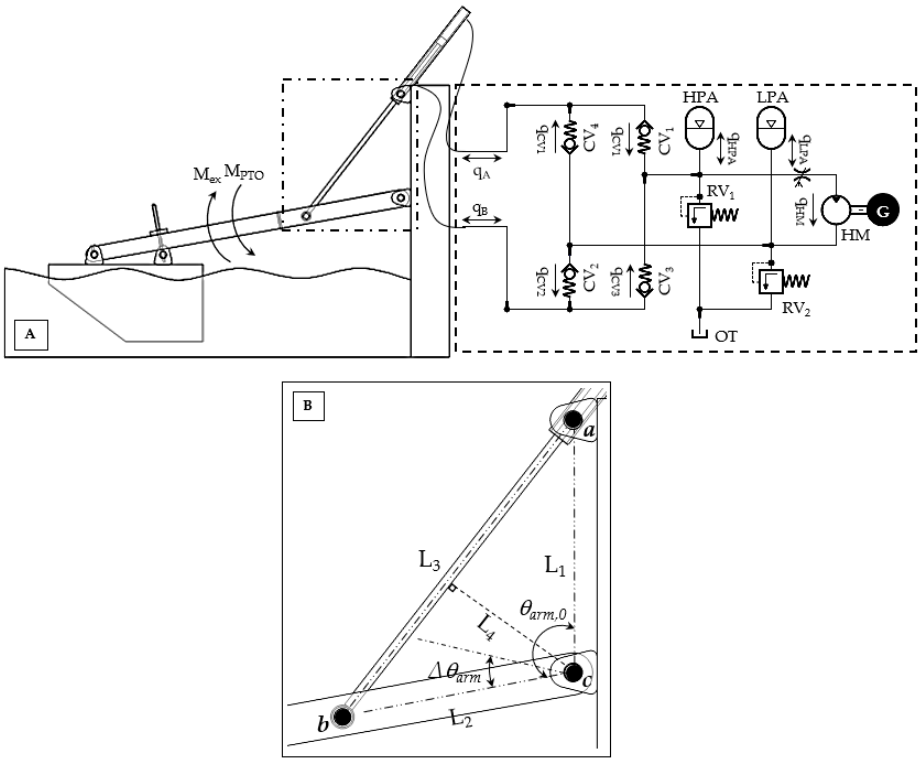

Figure 2. (**A**) Illustration of WEC with HPTO unit and (**B**) Configuration of hydraulic cylinder motion.

2.2. Hydraulic Power Take-off (HPTO) Mechanism

Figure 2A illustrates the considered HPTO unit, which includes a hydraulic actuator, set of control check valves (CV), high-pressure and low-pressure accumulator (HPA and LPA), hydraulic motor (HM) and electrical generator (G). In the HPTO unit, the large chamber of the hydraulic cylinder (chamber A) is connected to the CV_4 (outlet) and CV_1 (inlet), while the small chamber of DAC (chamber B) is connected to the CV_2 (outlet) and CV_3 (inlet), respectively. Meanwhile, HPA and LPA are placed at the inlet and outlet of the hydraulic motor. During the operation, the wave force generated from the passing ocean wave causes a floater to swing upward and downward repeatedly, as illustrated in Figure 2B. The mechanical force produced by the WEC device forces the rod and piston of the hydraulic cylinder at the specified velocity ($\dot{x}_p$) relatively subjected to the PTO load force. During the upward motion, the high-pressurised fluid in chamber A flows to the chamber B through CV_1, HPA, HM, LPA and CV_2. On the other hand, the process is vice-versa during downward motion, where high-pressure fluid in chamber B flows to chamber A through CV_3, HPA, HM, LPA and CV_4. The high-pressure fluid flows through HM lead to the HM, and G rotates simultaneously at the specified rotation speed (ω_G) subjected to the load torque of the G (τ_G). As a result, the usable electricity can be generated by the continuous motion of this mechanism.

In general, the behaviour of the HPTO unit is strongly nonlinear. Equations (6)–(21) theoretically explain the operation of the considered HPTO unit illustrated in Figure 2. According to Equation (6), the F_{PTO} from the HPTO unit applied to the WEC device depends on the pressure in both hydraulic chambers (p_A and p_B) and the effective piston area (A_P). Further, the effects of piston friction (F_{fric}) and initial force of rod, piston and oil (F_{in}) are also considered. These effects can be expressed using Equations (7) and (8), where η_{fric} is a friction coefficient, $\ddot{x}_p$ is the piston acceleration, g is a gravitational acceleration, M_p, M_r and M_{oil} are the mass of the piston, rod, and oil, respectively [12,36].

$$F_{PTO} = A_p(|p_A - p_B|) + F_{fric} + F_{in} \tag{6}$$

$$F_{fric} = \left|A_p(p_B - p_A)\right|\left(1 - \eta_{fric}\right) \tag{7}$$

$$F_{in} = \ddot{x}_p\left(M_p + M_r + M_{oil}\right) + \left(M_p + M_r\right)g \tag{8}$$

Since a double-acting-cylinder with a single rod piston is considered a hydraulic actuator, the F_{PTO} is unbalanced during the upward and downward motion of the WEC device due to the unbalanced pressure in both chambers of the hydraulic cylinder. Based on the configuration of the HPTO unit in Figure 2, the F_{PTO} during the upward movement is greater than the F_{PTO} during the downward movement. The dynamics of p_A and p_B can be described using a fluid continuity equation as in Equations (9) and (10) [12,37]. β_{eff}, q_A and q_B are the effective bulk modulus and the in/out volumetric flows in the hydraulic cylinder actuator. x_p, $\dot{x}_p$ and L are position, velocity and stroke length of the piston. $A_{p,A}$ and $A_{p,B}$ are the effective piston area in the hydraulic chamber A and B, that can be expressed by Equations (11) and (12), where the d_p and d_r are the diameter of the piston and rod, respectively.

$$\frac{d}{dt}p_A = \frac{\beta_{eff}}{A_{p,A}\left(L - x_p\right)}\left(q_A - \dot{x}_p A_{p,A}\right) \tag{9}$$

$$\frac{d}{dt}p_B = \frac{\beta_{eff}}{A_{p,B}\left(L - x_p\right)}\left(\dot{x}_p A_{p,B} - q_B\right) \tag{10}$$

$$A_{p,A} = \pi {d_p}^2/4 \tag{11}$$

$$A_{p,B} = \pi\left({d_p}^2 - {d_r}^2\right)/4 \tag{12}$$

For the check valve, the spring-loaded non-return valves are used in this HPTO model. The flow across the valve (q_{CV}) can be described by the orifice equation, as expressed in Equation (13), where C_d is the discharge coefficient, A_{CV} is the check valve opening area and ρ_{oil} is the fluid density. The p_{CVin} and p_{CVout} are the pressure at the inlet and outlet of the check valve [12,38].

$$q_{CV} = \begin{cases} C_d A_{CV} \sqrt{2|p_{CV_{in}} - p_{CV_{out}}|/\rho_{oil}}, \; if \; p_{CV_{in}} > p_{CV_{out}} \\ 0, \; else \end{cases} \tag{13}$$

Besides that, the gas compression and expansion in the HPA and LPA, which are based on the isentropic process, can be described according to Equations (14) and (15), respectively. Where p_{HPA}, p_{LPA}, $p_{0,HPA}$ and $p_{0,LPA}$ are the pressure and pre-charge pressure in the HPA and LPA. γ is the adiabatic index of the compressed gas in the HPA and LPA, while, $V_{HPA.}$, V_{LPA}, $V_{0,HPA}$ and $V_{0,LPA}$ are the initial and the instantaneous volume of gas in the HPA and LPA, respectively. The instantaneous volume of gas can be expressed by Equations (16) and (17), where q_{HPA} and q_{LPA} are the volumetric flow in the HPA and LPA.

$$p_{HPA} \cdot {V_{HPA}}^{\gamma} = p_{0,HPA} \cdot {V_{0,HPA}}^{\gamma} \tag{14}$$

$$p_{LPA} \cdot {V_{LPA}}^{\gamma} = p_{0,LPA} \cdot {V_{0,LPA}}^{\gamma} \tag{15}$$

$$V_{HPA}(t) = V_{0,HPA} - \int_0^t q_{HPA} dt \tag{16}$$

$$V_{LPA}(t) = V_{0,LPA} - \int_0^t q_{LPA} dt \tag{17}$$

Meanwhile, the fluid continuity in the HPTO model should satisfy the following equations:

$$q_{HPA} = q_{CV_1} + q_{CV_2} - q_{HM} \tag{18}$$

$$q_{LPA} = q_{CV_3} + q_{CV_4} - q_{HM} \tag{19}$$

where q_{HM} is the volumetric flow through the hydraulic motor. Here, q_{HM} is given by Equation (20), where D_{HM}, ω_{HM}, and $q_{HM,loss}$ are displacement, speed and volumetric flow losses of the hydraulic motor, respectively. The output torque of the hydraulic motor, τ_{HM} can be expressed by Equation (21), where Δp_{HM} is the pressure difference in the hydraulic motor.

$$q_{HM} = D_{HM}\omega_{HM} - q_{HM,loss} \tag{20}$$

$$\tau_{HM} = D_{HM}\Delta p_{HM} \tag{21}$$

Based on the theoretical descriptions provided in Equations (6)–(21), the most important component parameters, which influence the operation of the HPTO model can be defined as summarised in Table 1. The inaccuracy of the selected component parameters will reduce the HPTO unit's capability in converting the absorbed wave energy to electrical energy. Thus, the optimisation of these important component parameters using mathematical algorithms is considered in this study.

Table 1. Important component parameters of the HPTO system.

No.	Parameter Setting	Unit
1	Diameter of piston, d_p	m
2	Diameter of rod, d_r	m
3	Volume capacity of HPA, $V_{cap,HPA}$	L
4	Volume capacity of LPA, $V_{cap,LPA}$	L
5	Pre-charge gas pressure of HPA, $p_{0,HPA}$	Bar
6	Pre-charge gas pressure of LPA, $p_{0,LPA}$	Bar
7	Displacement of HM, D_{HM}.	cc/rev

3. Simulation Studies of WECs

3.1. Ocean Wave Input Data

A previous study reported that the ranges of the wave height (H_W) and wave period (T_W) at several locations in Terengganu, Malaysia, were equal to the range of 0.2–1.2 m and 2–8 s, respectively [39]. In addition, a further forecast analysis found that the most annual occurrences sea-state at the considered installed location were equal to 0.8 m and 2.5 s. From these statistical results, the regular and irregular wave inputs data were generated based on Airy's wave theory and Joint North Sea Wave Observation Project (JONSWAP) spectrum, as illustrated in Figure 3A,B, respectively. For the irregular wave data profile generation, the peak enhancement factor (γ) of JONSWAP was set to 2. Regular wave input profile data were used in determining the optimal parameters of the HPTO unit process. While the irregular wave input profile data were used to evaluate the effectiveness of the optimal HPTO unit in generating the electricity in inconsistent wave circumstances.

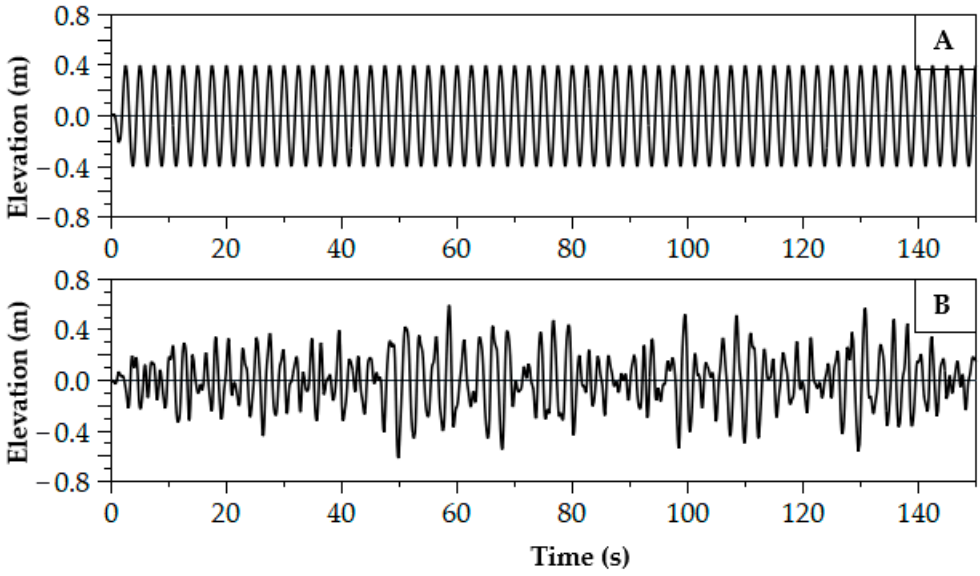

Figure 3. Ocean wave elevation inputs, (**A**) regular wave and (**B**) irregular wave.

3.2. Simulation Set-up of WEC with HPTO Unit Model

In the present study, the main specifications of the computer device that was used for the simulation studies are given in Table 2. As can be seen from Equations (1) and (2), the frequency domain analysis was required to determine the hydrodynamic parameters of the WEC device. Thus, hydrodynamic simulation of the WEC model was preliminarily performed using ANSYS/AQWA software. The hydrodynamic simulation method presented in [40,41] was considered. The results from the preliminary hydrodynamic simulation are presented in Figure 4. The parameters obtained from the hydrodynamic simulation were used to build the complete simulation model of WEC with the HPTO unit in *MATLAB*®® /Simulink software, as illustrated in Figure 5. A WEC model based on the linear wave motion, as mentioned in Equations (1)–(5), was developed using the function blocks.

Table 2. Main specifications of the computer device.

Item	Details
Type	Desktop
Windows	Windows 10 Pro
Memory (RAM)	12 GB
CPU	Intel (R) Core (TM) i7-9750H 2.60 GHz
MATLAB Version	R2019b

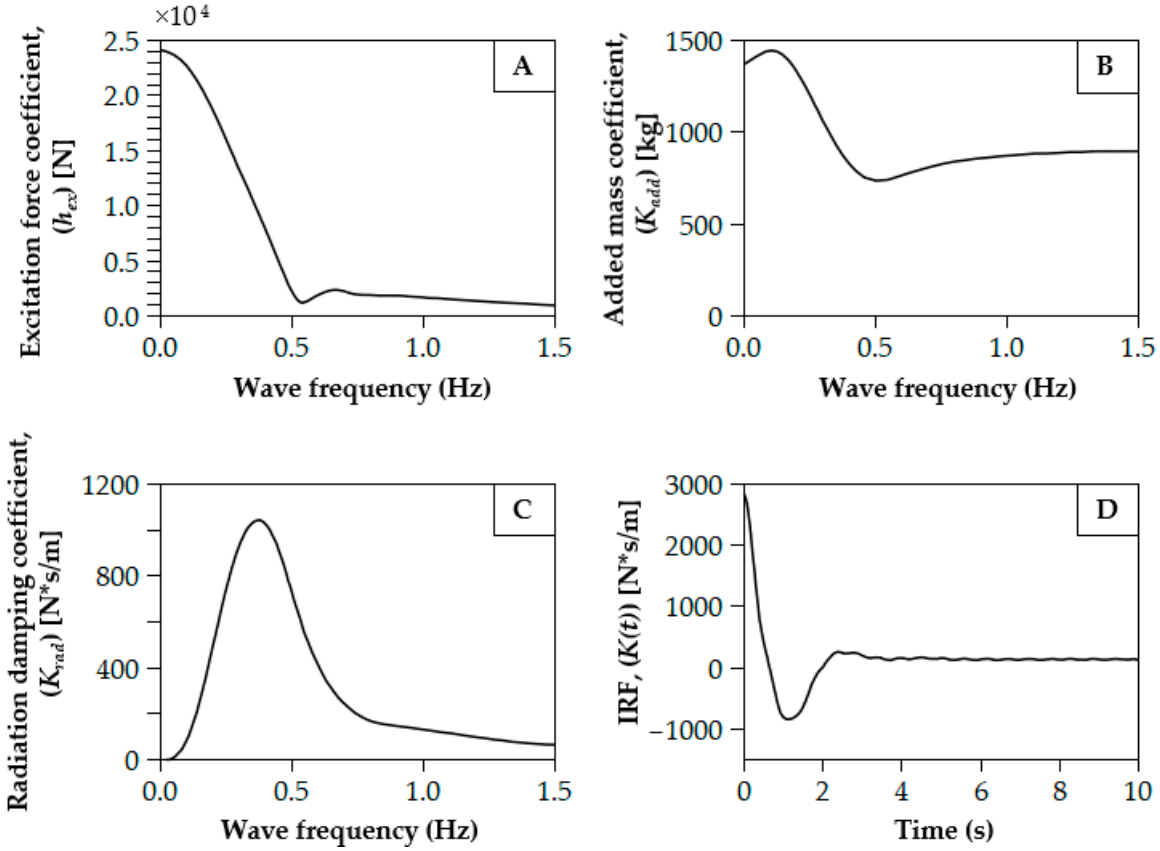

Figure 4. Hydrodynamic analysis parameters. (**A**) Excitation force coefficient, (**B**) added mass coefficient, (**C**) radiation damping coefficient, and (**D**) impulse response function.

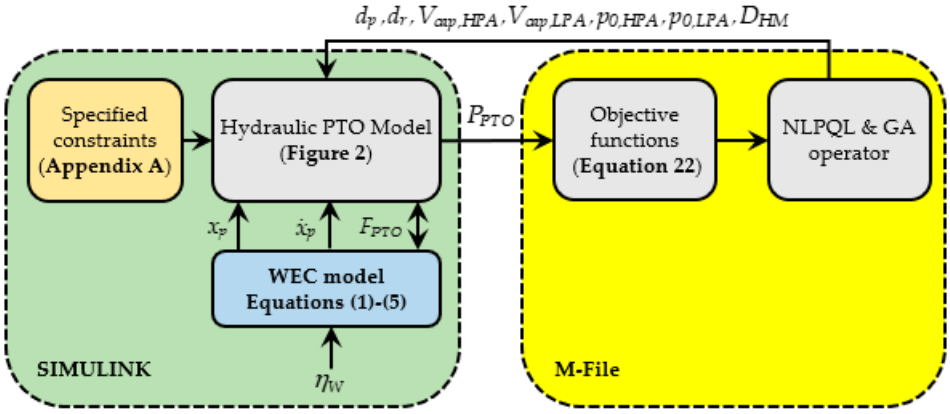

Figure 5. Illustration of simulation model set-up in MATLAB software.

Meanwhile, the HPTO model was developed using the hydraulic components in the Simscape Fluid toolbox, such as double hydraulic chamber single rod jack, hydraulic motor, hydraulic accumulator, hydraulic check valve with saturation, et cetera. The actual parameters of the hydraulic components from manufacturers were used to configure the HPTO model. Since the selection of the HPTO components was incredibly complex due to the variety of hydraulic products from the manufacturers and suppliers, the specification data of hydraulic components from a well-known manufacturer such as Parker Hannifin was considered, as summarised in Appendix A. The data in Appendix A were used as a guideline in determining the optimal configuration parameters of each element in the HPTO model simulation.

Furthermore, a simple dynamic sub-model of a rotary load was utilised to represent the permanent magnet synchronous generator (PMSG) unit. The generated electrical power output from the HPTO model was calculated based on the speed-power curve of PMSG, which was obtained from the manufacturer. In addition, the PTO force, hydraulic motor torque, hydraulic motor speed and electrical power were the acquired outputs from the HPTO model. The detailed specifications of each component that were used in the HPTO model are presented in Table 3.

Table 3. Technical specifications of the developed HPTO model.

Descriptions (Unit)	Value
Generator	
Rated power, P_{rated} (kW)	0.1
Rated speed, $\omega_{G,rated}$ (rpm)	200
Rated torque $\tau_{G,rated}$ (Nm)	6.0
Viscous friction coefficient, (Nm/rpm)	0.024
Moment of inertia, (kgm^2)	0.0036
Hydraulic cylinder	
Diameter of the piston, d_p (m)	0.035 *
Diameter of the piston rod, d_r (m)	0.025 *
Length of stroke, l_{stroke} (m)	0.3
HP accumulator	
Pre-charge gas pressure, $p_{0,HPA}$ (bar)	40 *
Volume capacity, $V_{cap,HPA}$ (L)	8 *
Adiabatic index, γ	1.4
LP accumulator	
Pre-charge gas pressure, $p_{0,LPA}$ (bar)	5 *
Volume capacity, $V_{cap,HPA}$ (L)	2 *
Adiabatic index, γ	1.4
Hydraulic motor	
Displacement, D_{HM} (cc/rev)	8 *
Oil properties	
Viscosity, Vis_{oil} (cSt)	50
Density, D_{oil} (kg/m^3)	850

* Initial value by manual estimation.

Simulation results of the WEC with non-optimal HPTO unit using the regular waves input profile data are shown in Figure 6. Figure 6A shows that the displacement of WEC was relatively lower than the wave displacement due to the PTO force applied to the WEC device. The PTO force profile applied to the WEC device is shown in Figure 6B. The figure shows that the PTO forces applied to the WEC device during the upward and downward motion were equal to 1.5 kN and 0.7 kN, respectively. Meanwhile, Figure 6C shows the electrical power generated from the non-optimal HPTO unit only can be reached up to an average of 71 W, which was 71% of its rated capacity.

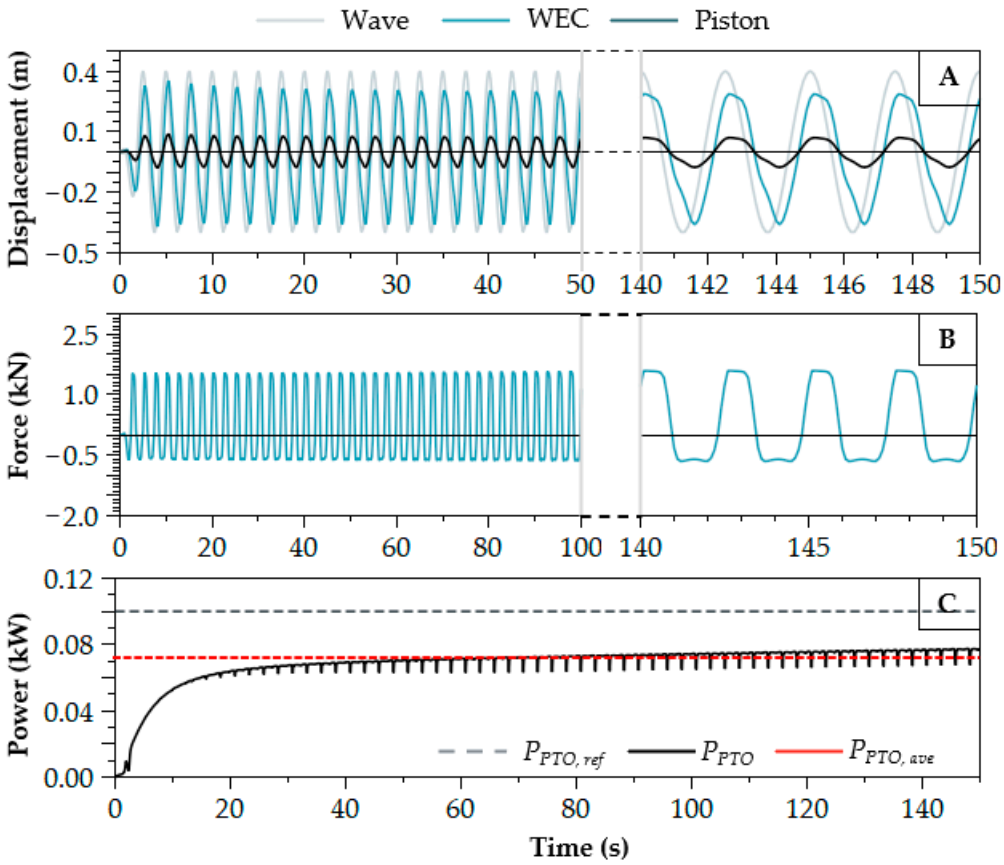

Figure 6. Preliminary simulation results of WEC with non-optimal power take-off (PTO) unit (H_W = 0.8, T_W = 2.5 s). (**A**) Wave, WEC and piston displacements, (**B**) PTO force, and (**C**) PTO power.

3.3. Optimisation of Configuration Parameter

As the sea state was relatively unstable throughout the year, a suitable HPTO unit was compulsory for a WEC device to ensure that the ocean wave energy can be maximally absorbed and converted to electrical energy. Conventionally, the optimal parameters of the HPTO unit were obtained by iteratively simulating the HPTO model using any sophisticated analysis software. In this process, the designer was required to manually specify a set of configuration parameters value, evaluate the HPTO unit model and analyse the PTO model output. Normally, this process may be repeated many times due to unsatisfactory results from the HPTO performance. Consequently, the designer again proposed a new set of HPTO parameters value based on experience and intuition, which probably will result in a better output of the HPTO model. This optimisation process will end when the time runs out. Unfortunately, sophisticated analysis software and high-speed computer technology were unable to help the designer in determining the optimal parameters of the HPTO unit using this technique.

Alternatively, the optimisation technique HPTO unit parameters using a computer algorithm was presented in this study. By using this technique, the designer was taken out from the trial-and-error loop process. The sophisticated computer was now utilised to conduct a complete determination process of the optimal configuration parameters. Through this technique, the designer workload can be reduced, in which the designer only focused on the interpretation of the optimisation results. Moreover, the determination of the optimal configuration parameters can be found in a shorter and more accurate time compared to the case using a conventional technique. In the algorithm-based optimisation technique, many kinds of algorithms can be applied to solve the optimisation problem.

In the present study, the simulation–optimisation using two major types of optimisation algorithms was explored in this present study. A specific objective function (OF) was designed to maximise the electrical energy generation of the HPTO unit, as described

in Equation (22). Here, $P_{PTO,ref}$ and P_{PTO} represented the desired and the actual electrical power output of the HPTO unit. The optimisation problem in Equation (22) was solved by two kinds of optimisation algorithms, i.e., NLPQL and GA. In order to provide a fair-ground for comparison between two optimisation algorithms, the same constraints, design parameters, and objective function were considered for both cases under study. The details of the considered algorithms are described in the following subsections.

$$OF(x) = min\left[\frac{\int_0^T \left(\left|P_{PTO}(t) - P_{ref}(t)\right|\right) dt}{\int_0^T P_{PTO,ref}(t)\, dt}\right] \quad (22)$$

3.3.1. Non-Evolutionary NLPQL-Based Optimisation

The NLPQL algorithm was a local optimiser and has the advantages of fast convergence and high-stability [42]. In several studies, the NLPQL-based optimisation was applied to solve and optimise various non-linear problems during the design stage [42–45]. Figure 7A shows the flowchart of the NLPQL-based optimisation technique. Initially, the NLPQL-based optimisation process was started by randomly generating the guest point of each study parameter (d_p, d_r, $p_{0,HPA}$, $V_{cap,HPA}$, $p_{0,LPA}$, $V_{cap,LPA}$, D_{HM}). Then, in the first iteration, the generated random guest point was chosen for each study parameter, and the HPTO model was then evaluated based on the objective function in Equation (22). The linear search calculation method was then implemented in order to determine the convergence satisfaction of the objective function. As presented in Figure 7A, the new iteration will be started if the objective function does not meet the convergence criterion. A new iteration was initially started to determine the new search direction and step size using the sequential quadratic programming (SQP) method. Then, the variables for each study parameters were determined based on the new search direction and step size. Finally, the Hessian approximation was updated by the modified BFGS-formula, as described in [42]. The parameters setting of the NLPQL-based optimisation is listed in Table 4. This process was repeated until the NLPQL algorithm met the termination accuracy.

Table 4. Parameters setting of NLPQL.

Setting	Value
Maximum number of function evaluations	7
Maximum number of iterations	100
Step size for finite difference step	0.001
Final accuracy	0.0001

3.3.2. Evolutionary GA-Based Optimisation

In contrast to the NLPQL, GA was an evolutionary algorithm that was inspired by the natural evolution process. GA has been effectively applied to a wide range of real-world problems. In this algorithm, the variables of the optimisation problem were coded in chromosomes. Figure 7B presents the flowchart of the GA pseudo-code. The GA-based optimisation process was initially started by randomly generating a population of chromosomes (study parameters: d_p, d_r, $p_{0,HPA}$, $V_{cap,HPA}$, $p_{0,LPA}$, $V_{cap,LPA}$, D_{HM}), as presented in Figure 7B. Thereafter, for the first iteration, the random values from the generated population were chosen for each study parameter. The HPTO model was then evaluated based on the objective function in Equation (22). The chromosomes of the population were then sorted according to the least cost or highest fitness. Some percentages of the best chromosomes were transferred directly to the next generation based on their merit. Then, three GA operators named as selection, crossover and mutation were implemented to manipulate the rest of the chromosomes for the next generation. During the selection rule, the parent's chromosome that contributed to the current population was selected for the next generation process. Then, pairs of selected parents were recombined by a crossover operator to produce new chromosomes. A mutation rule was then applied to the new

chromosomes to avoid the GA converging to the local optimum. Finally, this process was iterated until the satisfactory fitness level was reached. The parameters setting of GA was gathered in Table 5.

Table 5. Parameters setting of GA.

Setting	Value
Population size	50
Reproduction ratio (%)	80
Maximum number of generations	100
Mutation probability (%)	10
Mutation amplitude	0.1
Seed	1
Final accuracy	0.0001

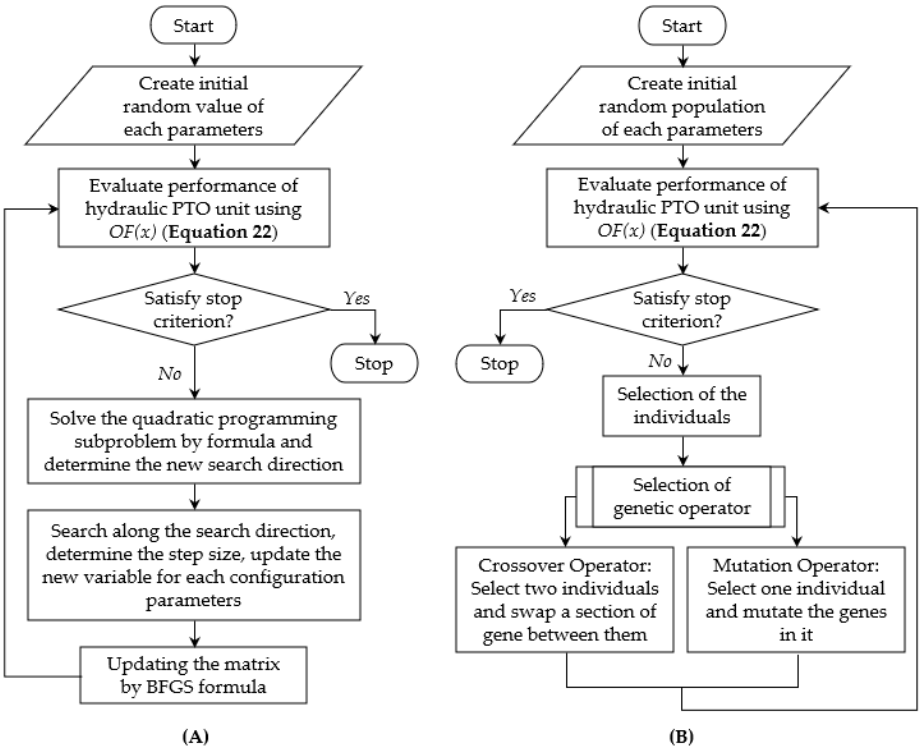

Figure 7. Optimisation procedures using (**A**) Non-Linear Programming by Quadratic Lagrangian (NLPQL) and (**B**) Genetic Algorithm (GA).

4. Results and Discussion

4.1. Comparisons between NLPQL and GA Optimisation of HPTO Unit

In order to evaluate the best optimisation approaches for the HPTO unit, a critical comparison analysis was performed. The comparison in terms of the final objective function, the best-estimated parameter values and the HPTO unit's performance were considered.

4.1.1. Chronological Variation of the Objective Function and Parameters Variables

Figures 8 and 9 depicted the chronological variation of the objective function and parameters variables with respect to the number of generations of the optimisation processes done by NLPQL and GA operators. The red vertical line in both figures indicated the optimisation process's termination at the lowest objective function value. The lowest objective function value was of interest for optimisation purposes in a feasible solution framework. Both of the optimisation processes were terminated after the algorithms

met the optimum point, which was determined based on the termination criterion (final accuracy), as previously mentioned in Tables 4 and 5.

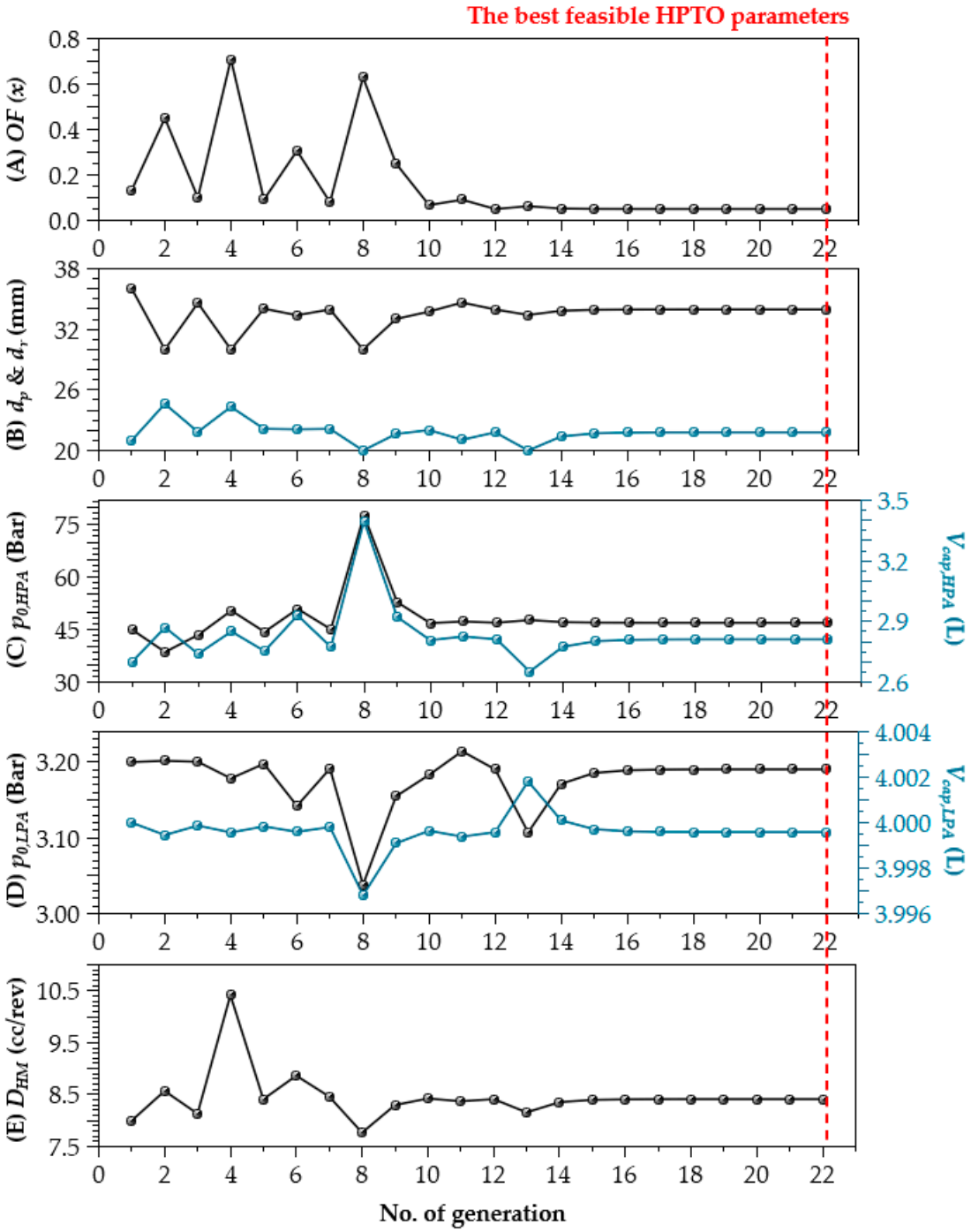

Figure 8. Chronological variation of (**A**) objective function, (**B**) diameter of piston and rod, (**C**) pre-charge gas pressure and capacity of HPA, (**D**) pre-charge gas pressure and capacity of LPA, and (**E**) displacement of HM for NLPQL algorithm.

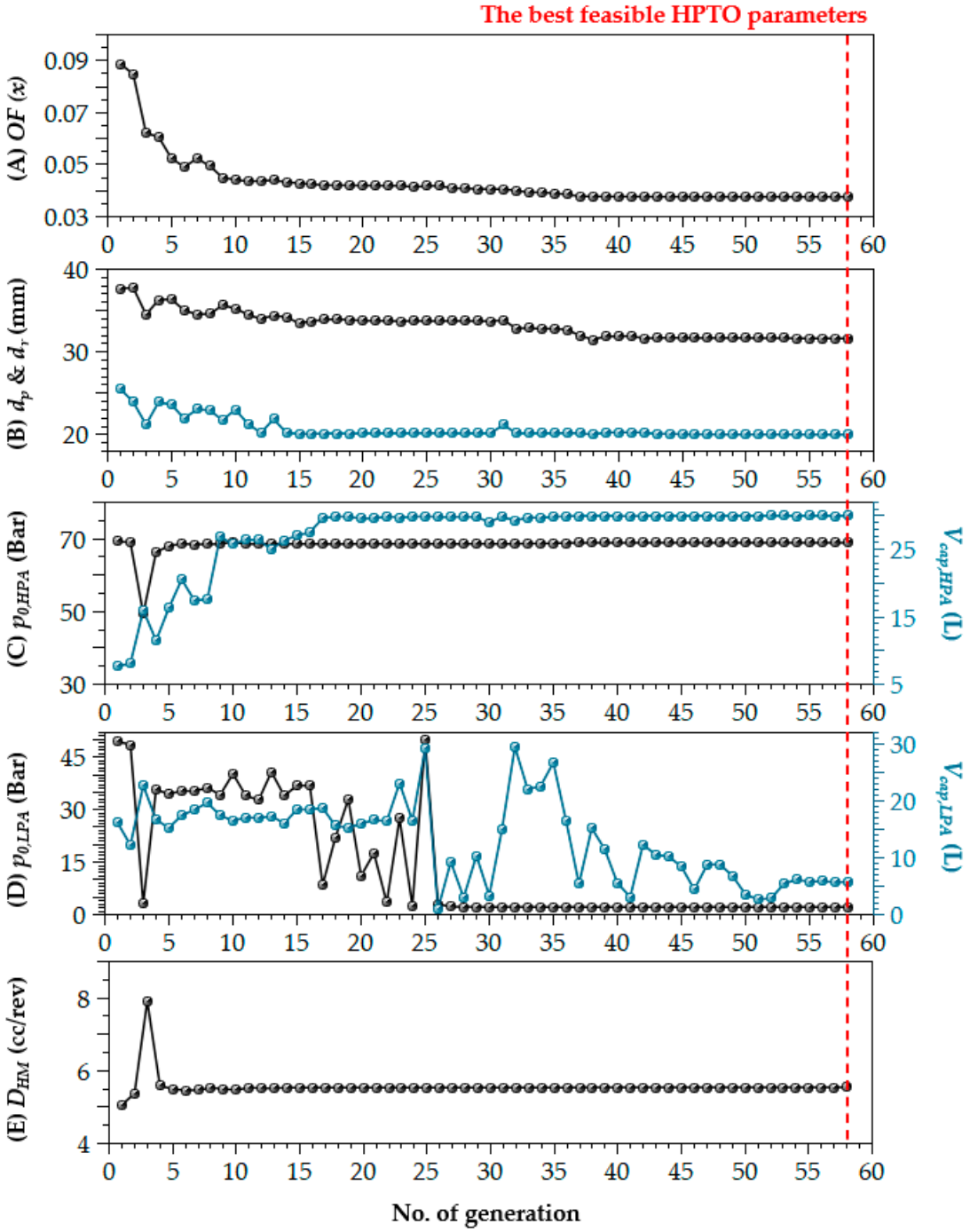

Figure 9. Chronological variation of (**A**) objective function, (**B**) diameter of piston and rod, (**C**) pre-charge gas pressure and capacity of HPA, (**D**) pre-charge gas pressure and capacity of LPA, and (**E**) displacement of HM for GA algorithm.

Figure 8A showed that the estimation process of the best configuration parameters was completed after the 22 number of iterations since the NLPQL operator had satisfied its accuracy requirement. The overall simulation–optimisation process using the NLPQL algorithm was carried out for 3237 s (approximately 53 m 57 s). As shown in the figure, the lowest objective function value at 22 iterations was obtained at 0.0492. Meanwhile, 56 numbers of iterations were needed to find the optimum case by the GA operator, as exhibited in Figure 9A. A complete simulation–optimisation process by the GA operator was performed for 7 h and 32 min. The lowest objective function was obtained equal to 0.0375, as illustrated in Figure 9A. Besides that, Figure 8B–E showed the chronological variation of the HPTO parameters throughout the optimisation process by the NLPQL algorithm. From

these figures, the HPTO parameters seemed to approach the optimum conditions starting from 14 number of iterations. On the other hand, for the GA optimisation, Figure 9B–E showed that some of the HPTO parameters reached the best condition after 5 iterations.

In summary, the comparison of the chronological results of both optimisation approaches in Figure 8, and Figure 9 found that the optimisation using the NLPQL algorithm was much faster than the GA optimisation case. The reason was that since the NLPQL was the local optimisation approach, this algorithm depended on the initial point of each HPTO parameter. As reported in [42], the numerical test showed that different initial points required different time consumed and would give different optimal results. In contrast to the NLPQL algorithm, since the GA is a global algorithm, it takes more time in its exploration and exploitation processes that consider more points in search space in order to find the optimum condition. Thus, it returns more accurate and reliable results as depicted in Figure 9. In order to improve the performance of the NLPQL algorithm, the hybridisation of the NLPQL algorithm with the other global optimisation operators can be considered, as presented in [46]. In [46], the optimal starting points of the NLPQL algorithm were set by GA, and better optimum results have turned up.

4.1.2. Best Estimated Parameters

Table 6 presents the best configuration parameters sets of the HPTO unit that were successfully estimated using NLPQL and GA optimisation approaches. As shown in the table, the d_p and d_r parameters of the hydraulic cylinder were estimated at 3% and 12.8% smaller than their initial values for the NLPQL case, which equaled to 34.9 mm and 21.8 mm, respectively. For the GA case, the d_p and d_r were estimated closely to their minimum constraints, which equal to 37.6 mm and 10 mm. Apart from that, the data in Table 6 reported that the best-estimated values of the $p_{0,HPA,}$ and $V_{cap,HPA}$ from the NLPQL, and GA optimisation were significantly different from their initial condition. The optimal value of $p_{0,HPA}$ was estimated larger than its initial value for both cases. While, for the $V_{cap,HPA}$, Table 6 clearly shows that the best values of $V_{cap,HPA}$ were estimated 65% lower and 275% larger than its initial value for the NLPQL and GA cases. For the $p_{0,LPA}$ and $V_{cap,LPA}$, the best-estimated values were not too significantly different from their initial values for both cases. Furthermore, it can be found in Table 6 that the best values of D_{HM} were significantly different between both optimisation cases. The result from the table shows that the GA operator successfully estimated a smaller value of D_{HM} compared to the NLPQL case.

In summary, based on the comparison of best configuration parameters estimated from both optimisation approaches, a few preliminary conclusions in terms of physical size, cost of the HPTO unit and others can be drawn. Practically, the physical size, weight and cost of the HPTO unit depend on its configuration parameters. Based on the results in Table 6, it can be preliminarily concluded that the physical size and weight of the HPTO unit for the NLPQL approach were much smaller than the GA approach case. This was due to the larger capacity of HPA as estimated by the GA approach. The physical size and weight of the HPTO unit were vital to being reduced since they can influence the complete design of the WECs, as reported in [13]. Moreover, the configuration parameters also influenced the total cost of the HPTO unit. As reported in [10], the hydraulic accumulator and the hydraulic motor were the most expensive HPTO unit components. Thus, from Table 6, it can be concluded that the overall cost of the WECs from the NLPQL optimisation approach was much lower than the GA case.

Table 6. Best configuration parameters from NLPQL and GA parameter estimation approaches.

Parameter (Unit)	Non-Optimal Case	Optimal Case by	
		NLPQL	GA
Hydraulic cylinder			
Diameter of piston, d_p (mm)	36	34.9	31.6
Diameter of piston rod, d_r (mm)	25	21.8	20.0
HP accumulator			
Pre-charge gas pressure, $p_{0,HPA}$ (bar)	40	46.9	68.9
Volume capacity, $V_{cap,HPA}$ (L)	8	2.8	30.0
LP accumulator			
Pre-charge gas pressure, $p_{0,LPA}$ (bar)	5	3.2	2.2
Volume capacity, $V_{cap,LPA}$ (L)	2	4.0	5.8
Hydraulic motor			
Displacement, D_{HM} (cc/rev)	8	8.4	5.5

4.1.3. Operational Behaviour of the HPTO Unit

Table 7 compares the operational behaviour of the HPTO unit for the non-optimal, NLPQL-optimal, and GA-optimal cases. By comparing the data in Table 7 and Appendix A, the HPTO unit's operations were satisfied with its operational constraints for all cases. As reported in Table 7, the overall operating pressure of the HPTO unit increased for both optimal cases. For example, the operating pressures of the hydraulic cylinder chambers for the NLPQL-optimal case increased by 8.6% (side A) and 8.8% (side B). While, for the GA-optimal case, the operating pressures of the hydraulic cylinder increased by 56.6% (side A) and 56.8% (side B) from the non-optimal case, respectively. Besides that, the pressures in the HPA for both cases also increased up to 10.1% and 60.8%, respectively. The hydraulic motor pressure also significantly increased by 9.4% and 60% for both cases, up to 47.5 bar and 69.8 bar.

Table 7. Comparison of the operational behaviour of the HPTO unit for non-optimal, NLPQL-optimal, and GA-optimal cases.

Descriptions (Unit)		Non-Optimal Case	Optimal Case by	
			NLPQL	GA
Hydraulic cylinder				
Max. operating pressure, (bar)	Side A	46.48	50.5	72.8
	Side B	46.40	50.5	72.8
Max. operating flow rate, (L/min)	Side A (In)	2.75	3.49	2.71
	Side A (Out)	4.73	4.29	4.05
	Side B (In)	2.10	2.08	2.33
	Side B (Out)	2.07	2.23	2.25
HP accumulator				
Max. operating pressure, (bar)		43.4	47.8	69.8
Max. operating flow rate, (L/min)	In	3.78	3.23	3.06
	Out	1.36	1.66	1.10
LP accumulator				
Max. operating pressure, (bar)		5.05	3.25	2.61
Max. operating flow rate, (L/min)	In	1.28	1.66	1.09
	Out	1.30	1.82	0
Hydraulic motor				
Max. operating pressure, (bar)	Inlet	43.4	47.5	69.8
	Outlet	5.03	3.25	2.63
Max. operating flow rate, (L/min)		5.03	1.67	1.10
Max. operating speed, (rpm)		174	202	204
Max. operating torque, (Nm)		5.24	6.04	6.05

The increasing pressure in the HPTO unit significantly increased the speed and torque of the hydraulic motor. As depicted in Table 7, the hydraulic motor speed and torque increased to its rated (200 rpm, 6 Nm) for both cases. In short, the results in Table 7 clearly show that the operational speed and torque of the hydraulic were influenced by the pressure of the other components in the HPTO unit. Thus, the presented results in Table 7 proved that the optimisation process by NLPQL and GA were highly effective in estimating the best component parameters of the HPTO unit.

4.1.4. Performance of the WECs

Technically, the force of the HPTO unit was directly proportional to its operational pressure [15,37]. Since the HPTO unit's pressure significantly increased, the HPTO force applied to the WEC device also increased, as depicted in Figure 10. Comparing Figure 10 with Figure 6B showed that the HPTO force applied to the WEC obviously increased for both cases. As depicted in Figure 10A, the HPTO forces applied to the WEC for the NLPQL case can be reached up to 1.65 kN (upward) and 0.78 kN (downward). While, for the GA-optimal case, the HPTO forces applied to the WEC can be reached up to 2.3 kN (upward) and 1.2 kN (downward), respectively. The results clearly showed that the overall HPTO force applied to the WEC device for the GA-optimal case was significantly larger than the HPTO force in the NLPQL case. This significant difference was attributed due to the larger pre-charge gas pressure and volume capacity of the HPA in the HPTO unit for the GA-optimal case, as depicted in Table 6. A larger pre-charge gas pressure required a more massive flow of high-pressure fluid [10]. In addition, from both figures, it can be seen that the HPTO forces applied to the WEC device during the upward movement were larger compared to the downward movement for both cases. This was due to the unsymmetrical double-acting hydraulic cylinder used in the HPTO unit. Since the hydraulic cylinder chambers were unsymmetrical, the fluid pressure in the chamber, which comprises a large effective piston area, was higher than the fluid pressure in the small effective area chamber, as clearly described in [10].

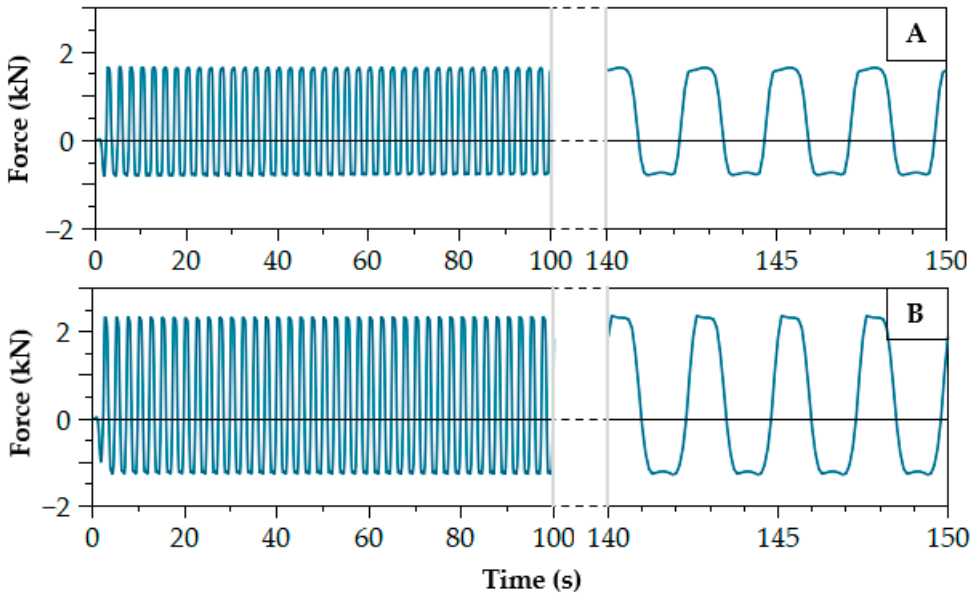

Figure 10. HPTO force applied to the WEC device (H_W = 0.8, T_W = 2.5 s), (**A**) NLPQL and (**B**) GA cases.

Furthermore, the HPTO force's effect on the displacement of the WEC device and hydraulic cylinder piston can be seen in Figure 11. Figure 11A,B illustrated the displacement of the wave, WEC, and hydraulic cylinder piston during the HPTO unit operation for both optimal cases. In Figure 11A, it was depicted that the average displacements of the WEC device and hydraulic cylinder piston for the NLPQL-optimal were 77.5% and 19.3% of the average wave elevation. Meanwhile, for the GA-optimal case, the average displacement of

the WEC device and hydraulic cylinder piston was 65% and 16% of average wave elevation. The comparison of the results in Figures 6A and 11 showed that the displacement of the WEC device and hydraulic cylinder piston was slightly reduced for the NLPQL-optimal and GA-optimal cases. The reduction was due to the larger HPTO force applied to the WEC device in both cases. In addition, the comparison of Figure 11A,B showed that the average displacement of the WEC device and hydraulic cylinder piston for GA-optimal was less than the NLPQL-optimal case.

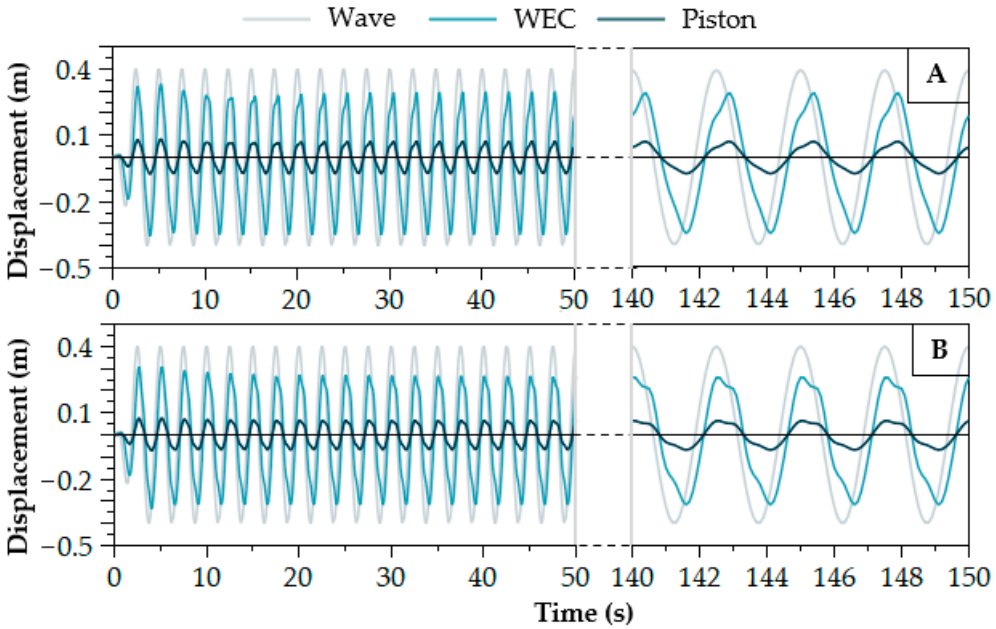

Figure 11. Displacement of the wave, WEC, and piston for three different cases (H_W = 0.8, T_W = 2.5 s), (**A**) NLPQL and (**B**) GA cases.

Apart from that, Figure 12 illustrated the comparison of the electrical power generation profiles of WECs for both optimal cases. Comparing the results in Figure 12 with Figure 6C, the overall electrical power generated from the HPTO unit optimised by NLPQL and GA approaches was successfully enhanced. For the non-optimal case, the electrical power profile in Figure 6C clearly indicated that the electrical power generated from the HPTO unit was lower than its rated capacity. Figure 6C showed the electrical power generated from the non-optimal HPTO was up to 71% (71 W) of its rated capacity. In contrast to both optimal cases. From Figure 12, the result showed the electrical generated output of HPTO was close to its rated capacity. The average electrical power generated from the HPTO unit for the NLPQL-optimal and GA-optimal cases was calculated up to 96% (96 W) and 97% (97 W) rated capacity, respectively. The comparison results in Figure 12 also showed that the electrical power generated from the HPTO unit of the GA-optimal case fluctuated less compared to the NLPQL-optimal case. This was due to the larger HPA used in the HPTO unit of the GA-optimal case. In addition, both of the optimal HPTO units reached their steady-state condition around 80 s.

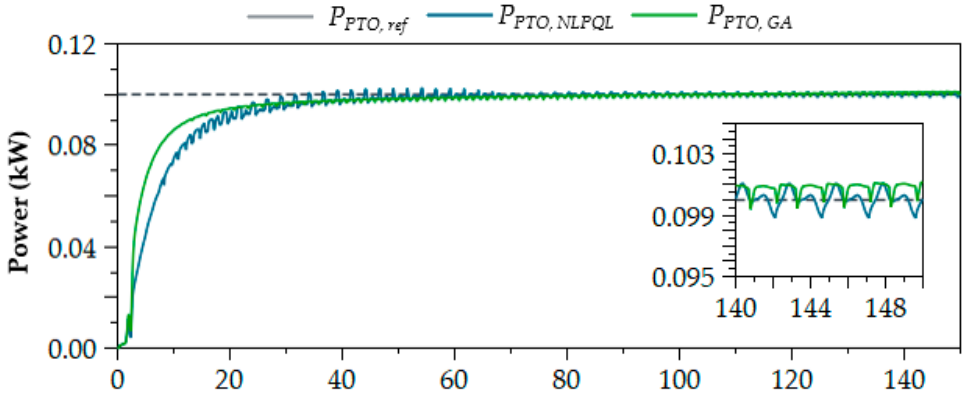

Figure 12. Comparison of electrical power generated from the best HPTO unit estimated by NLPQL and GA optimisations (H_W = 0.8, T_W = 2.5 s).

4.2. Evaluations of Optimal WECs Using Irregular Wave Data

The optimal HPTO units obtained from the optimisation processes were evaluated using irregular wave elevation input in order to evaluate their performance in generating the electricity in irregular wave circumstances. The results in Figure 13 provided the hydraulic cylinder piston responses for both cases. The figure showed that the displacement of the hydraulic cylinder piston for GA-optimal was smaller than the NLPQL-optimal case. This was due to the different pressures in the hydraulic cylinder chambers, as shown in Figure 14. Figure 14A showed that the reciprocating motions of the piston for the NLQPL case produced high-pressure liquid in both hydraulic cylinder chambers that reached up to 54 Bar. At the same time, the pressure of the hydraulic cylinder chamber for the GA case reached up to 75 Bar. The pressure difference for both cases was due to the difference in the HPTO unit's parameter design.

The high-pressure liquid produced in the hydraulic cylinder chamber then flowed to HPA and hydraulic motor. The HPA was used as liquid energy storage to smooth out pressure fluctuation in the HPTO unit. Thus, the liquid's pressure, which exceeded the HPA pre-charge pressure setting, was accumulated in the HPA ballast. In contrast, the HPA released the high-pressure liquid stored in its ballast when the HPTO system's pressure was lower than its pre-charge pressure setting. Figure 15 showed the pressure of the HPA for both optimal cases. For both cases, the pre-charge pressures of HPA were set to 46.9 Bar and 68.9 Bar, as previously given in Table 6. In Figure 15A, the pressure of the HPA reached up to 49 Bar, which was 4.5% higher than its pre-charge pressure setting several times. For the GA case, the highest pressure of the HPA can be reached up to 69.01 Bar, which was 0.16% higher than its pre-charge pressure setting, as depicted in Figure 15B. The difference in the pressure variation rate of HPA in both cases was due to the different HPA volume capacity. As given in Table 6, the volume capacity of HPA for the GA-optimal case was larger than the NLPQL-optimal case. In addition, the comparison of results in Figure 15A,B showed that the high-pressure liquid accumulation was more often for the GA-optimal case. This was due to a larger volume capacity of HPA used in the HPTO unit.

The smoothing effects of the HPA unit on the pressure in the HPTO unit for both optimal cases can be clearly seen in Figure 16. Figure 16A,B showed the smoothed pressure of the hydraulic motor for both cases. The comparison results in Figure 16A,B showed that the smoothing effect of the hydraulic motor pressure for the GA-optimal case was higher than the NLPQL-optimal case. It can be seen from the figures, the pressure of the hydraulic motor fluctuated less for the GA-optimal case compared to the NLPQL-optimal case. However, at the initial state of both cases, the hydraulic motor's pressure was more fluctuating due to insufficient energy stored in the HPA, as depicted in Figure 15. In addition, Figure 17 illustrated the comparison of the hydraulic motor speed for both cases. From the figure, the average speed of the hydraulic motor for the GA-optimal case was higher than the NLQPL-optimal case, which was 163 rpm instead of 137 rpm.

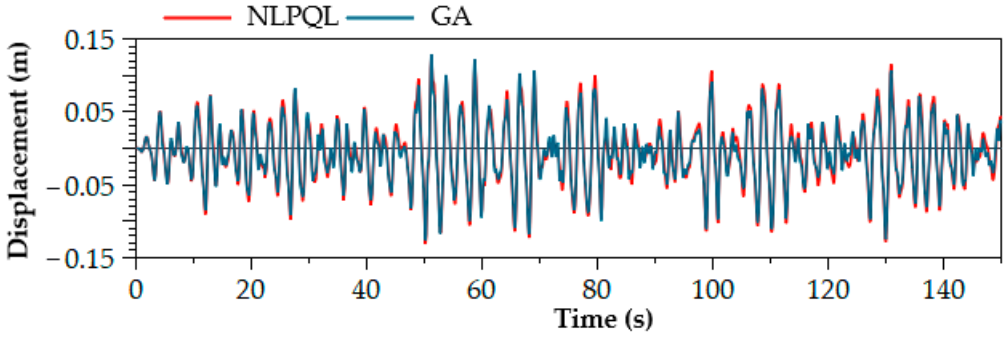

Figure 13. Displacement of hydraulic cylinder piston of HPTO unit (H_W = 0.8, T_W = 2.5 s).

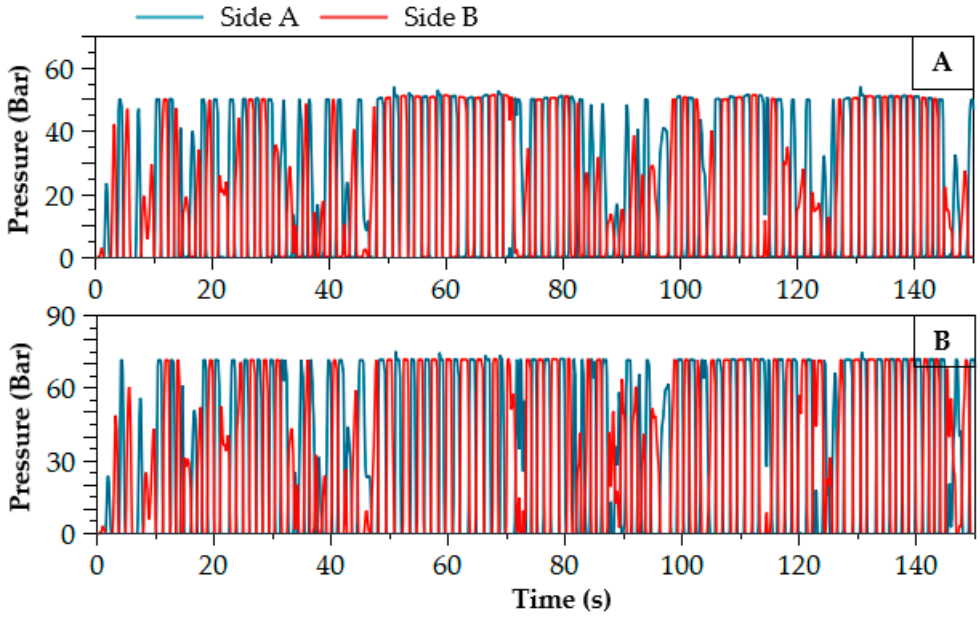

Figure 14. The pressure of the hydraulic cylinder chamber of HPTO unit (H_W = 0.8, T_W = 2.5 s), (**A**) NLPQL and (**B**) GA cases.

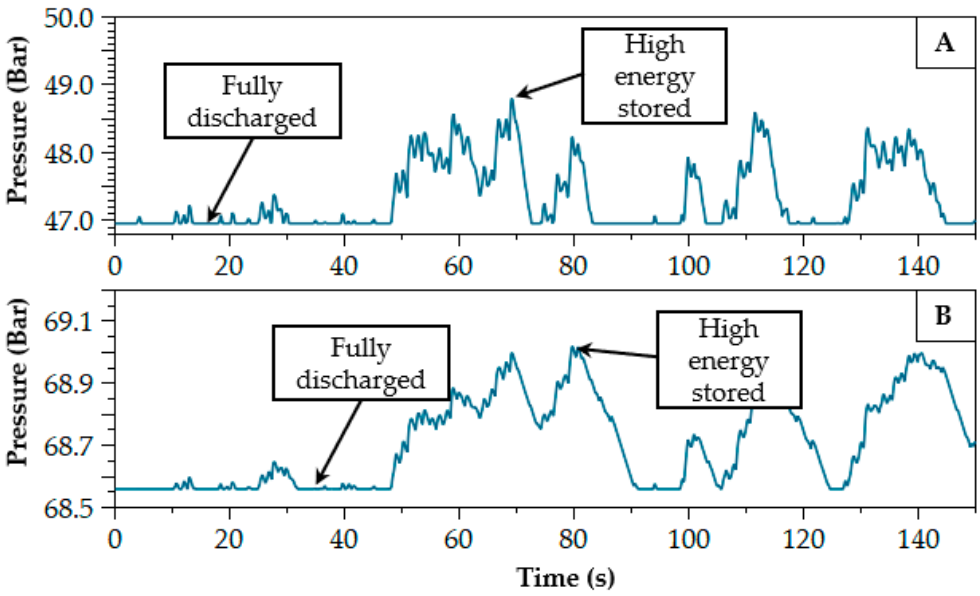

Figure 15. Pressure of high-pressure accumulator of HPTO unit (H_W = 0.8, T_W = 2.5 s), (**A**) NLPQL and (**B**) GA cases.

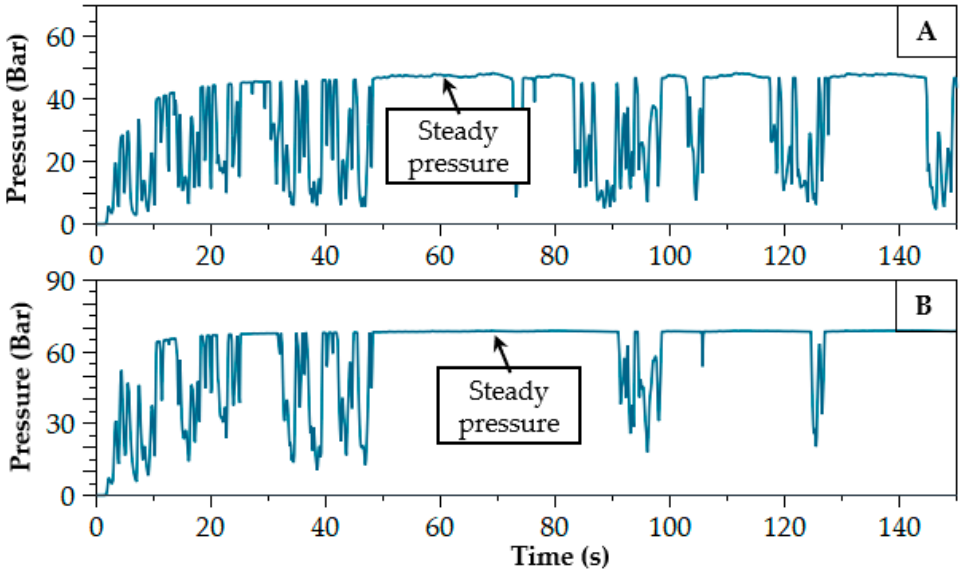

Figure 16. The pressure of hydraulic motor of HPTO unit (H_W = 0.8, T_W = 2.5 s), (**A**) NLPQL and (**B**) GA cases.

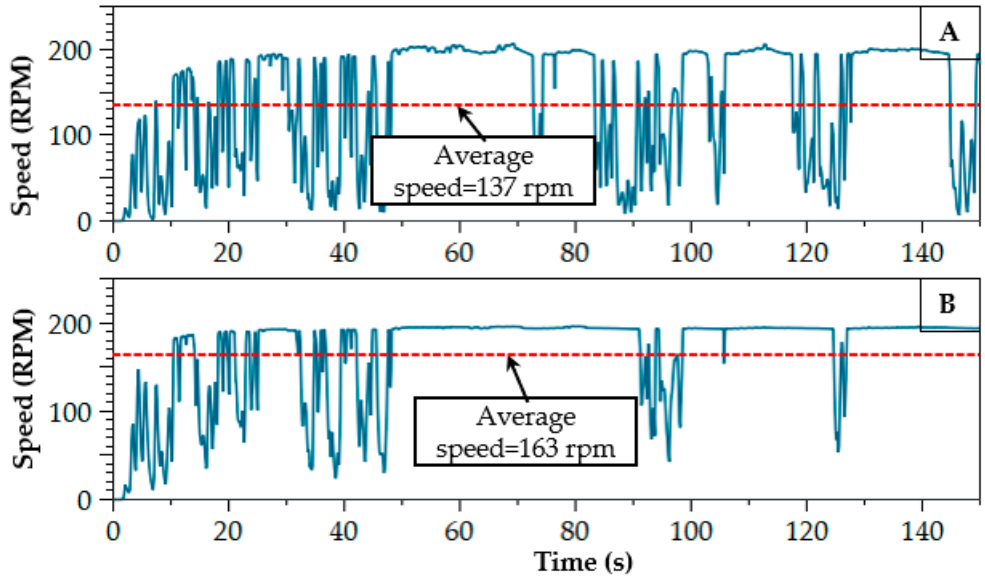

Figure 17. Speed of hydraulic motor of HPTO unit (H_W = 0.8, T_W = 2.5 s), (**A**) NLPQL and (**B**) GA cases.

Figure 18A–C presented the electrical power profiles of the HPTO unit for the non-optimal, NLPQL-optimal and GA-optimal cases. For the non-optimal case, the average electrical power generated from the PMSG generator in the HPTO unit was equal to 55 W, which was only 55% of its rated capacity, as shown in Figure 18A. For this case, the highest electrical power that was generated only reached up to 71 W. This was significantly different for the cases of the optimal HPTO unit optimised by NLPQL and GA approaches. It can be seen in Figure 18B,C, both optimal HPTO units capable of generating electricity of up to an average of 62 W and 77 W, which was 62% and 77% of its rated capacity, respectively.

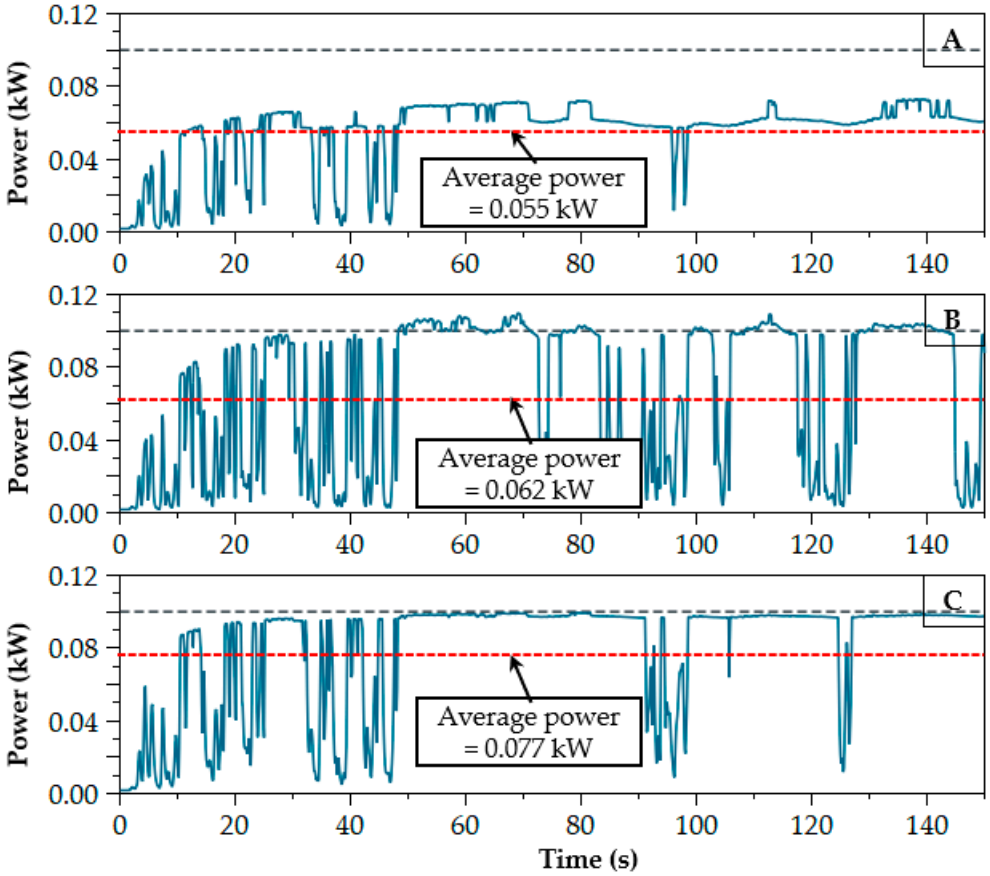

Figure 18. Comparison of electrical power generated from the best HPTO unit in irregular wave condition (H_W = 0.8, T_W = 2.5 s), (**A**) Non-optimal, (**B**) NLPQL-optimal, and (**C**) GA-optimal cases.

5. Conclusions

A comprehensive study was conducted to estimate the configuration parameters of the HPTO unit for a wave energy conversion device using a non-evolutionary NLPQL and evolutionary genetic algorithm. Seven important configuration parameters of the HPTO unit were considered in this optimisation study. The simulation–optimisation of HPTO model parameters was performed using MATLAB®® /Simulink software. The optimisation function problem was designed to maximise the output power generated from the HPTO unit. The optimal HPTO unit was then evaluated using irregular wave input to evaluate its performance in irregular circumstances. From the simulation studies, the key results can be listed as follows:

- The simulation–optimisation using the NLPQL algorithm was completed after the 22 number of iterations with the duration of 3237 s (approximately 53 m 57 s) after the NLPQL operator had satisfied its accuracy requirement. Importantly, the overall performance of HPTO has significantly improved up to 96% in regular wave conditions.
- The simulation–optimisation duration using the GA technique is longer than the NLPQL approach, which was completed after 7 h and 32 min. However, the overall performance of HPTO has significantly improved up to 97% in regular wave conditions.
- The HPTO unit estimated by the NLPQL approach is much smaller in terms of size, weight and cost compared to the GA approach. Thus, the HPTO unit's cost estimated by NLPQL is cheaper than the HPTO unit cost estimated by the GA approach.
- The results show that both optimal HPTO units can generate electricity up to 62% and 77% of rated capacity in irregular wave circumstances.
- In conclusion, both of the optimisation approaches were effective in determining the optimal parameters of the HPTO unit. For the sake of quickness, the NLPQL

approach is more relevant. While, for the sake of effectiveness, the GA approach is more recommended.

The simulation–optimisation framework presented may help the engineers and researchers of WECs to design a reliable and high-efficiency HPTO unit for wave energy converter devices. It is suggested that further researches should be conducted in the following areas:

- Further experimental validation of the best estimated HPTO unit is needed to verify the accuracy of the developed model simulation.
- The simulation–optimisation of the HPTO unit using other types of the optimisation algorithm, such as Particle Swarm Optimization, Gravitational Search Algorithm, et cetera, needs to be explored to achieve a good trade-off between cost and performance.
- The simulation–optimisation using other software types, such as Simcenter Amesim software invented by Siemens, is highly recommended.

Author Contributions: M.A.J., conceptualisation, methodology, software, data curation, analysis, writing—original draft; M.Z.I., writing—review and editing and supervision, project administration, funding acquisition; M.Z.D., conceptualisation, methodology, writing—review and editing and supervision; Z.M.Y., software, data curation, analysis and writing—original draft; A.A. data curation, analysis and writing—review and editing. All authors have read and agreed to the published version of the manuscript.

Funding: This project was funded by the Ministry of Higher Education (MOHE) under Fundamental Research Grant Scheme (FRGS/1/2019/TK07/UMT/01/1).

Acknowledgments: The authors would like to thank the Ministry of Higher Education (MOHE) and Universiti Malaysia Terengganu (UMT) for financial support for this research.

Conflicts of Interest: The authors declare no conflict of interest.

Abbreviations

ACO	Ant Colony Optimization
CFD	Computational Fluid Dynamics
CV	Check Valve
GA	Genetic Algorithm
GSA	Gravitational Search Algorithm
HM	Hydraulic Motor
HPA	High-Pressure Accumulator
HPTO	Hydraulic Power Take-Off
JONSWAP	Joint North Sea Wave Observation Project
LPA	Low-Pressure Accumulator
NLPQL	Non-Linear Programming by Quadratic Lagrangian
OF	Objective Function
PMSG	Permanent Magnet Synchronous Generator
PSO	Particle Swarm Optimization
PTO	Power Take-Off
SOC	State-Of-Charge
SQP	Sequential Quadratic Programming
TS	Tabu Search
WAB	Wave-Activated-Body
WEC	Wave Energy Converter
WECs	Wave Energy Converters

Appendix A

Table A1. Specifications of hydraulic components from Parker Hannifin Manufacturer.

HPTO Component (Unit)	Ranges		Ref.
	Minimum	Maximum	
Hydraulic cylinder [a]			[47]
Available piston diameter, (mm)	30	203	
Available rod diameter, (mm)	10	140	
Operating pressure, (bar)	0	207	
Operating flow rate, (L/min)	0	900	
HP accumulator [b]			[48]
Available nominal volume, (L)	0.2	57	
Operating pressure, (bar)	0	690	
Operating flow rate, (L/min)	0	900	
LP accumulator [c]			[49]
Available nominal volume, (L)	0	565	
Operating pressure, (bar)	0	80	
Operating flow rate, (L/min)	0	3000	
Hydraulic motor [d]			[50]
Available motor displacement, (cc/rev)	20	23,034	
Operating pressure, (bar)	0	420	
Operating speed, (rpm)	0	1000	
Operating flow rate, (L/min)	0	200	
Operating torque, (Nm)	0	1428	

[a] Heavy Duty Roundline Welded Series, [b] High-Pressure Bladder Accumulator Series, [c] Low-Pressure Bladder Accumulator Series, [d] High Torque Radial Piston Motors Series.

References

1. Sang, Y.; Karayaka, H.B.; Yan, Y.; Yilmaz, N.; Souders, D. Ocean (Marine) Energy. In *Comprehensive Energy Systems*; Elsevier: Amsterdam, The Netherlands, 2018; Volumes 1–5, pp. 733–769, ISBN 9780128095973.
2. Mustapa, M.A.; Yaakob, O.B.; Ahmed, Y.M.; Rheem, C.K.; Koh, K.K.; Adnan, F.A. Wave energy device and breakwater integration: A review. *Renew. Sustain. Energy Rev.* **2017**, *77*, 43–58. [CrossRef]
3. de Falcão, A.F.O. Wave energy utilization: A review of the technologies. *Renew. Sustain. Energy Rev.* **2010**, *14*, 899–918. [CrossRef]
4. Titah-Benbouzid, H.; Benbouzid, M. An up-to-date technologies review and evaluation of wave energy converters. *Int. Rev. Electr. Eng.* **2015**, *10*, 52–61. [CrossRef]
5. Rusu, E.; Onea, F. A review of the technologies for wave energy extraction. *Clean Energy* **2018**, *2*, 10–19. [CrossRef]
6. Al Shami, E.; Zhang, R.; Wang, X. Point absorber wave energy harvesters: A review of recent developments. *Energies* **2019**, *12*, 47. [CrossRef]
7. Têtu, A. *Power Take-Off Systems for WECs*; Springer: Cham, Switzerland, 2017; pp. 203–220.
8. Kukner, A.; Erselcan, İ.Ö. A review of power take-off systems employed in wave energy. *J. Nav. Sci. Eng.* **2014**, *10*, 32–44.
9. Gaspar, J.F.; Calvário, M.; Kamarlouei, M.; Guedes Soares, C. Power take-off concept for wave energy converters based on oil-hydraulic transformer units. *Renew. Energy* **2016**, *86*, 1232–1246. [CrossRef]
10. Jusoh, M.A.; Ibrahim, M.Z.; Daud, M.Z.; Albani, A.; Yusop, Z.M. Hydraulic power take-off concepts for wave energy conversion system: A review. *Energies* **2019**, *12*, 4510. [CrossRef]
11. Galván-Pozos, D.E.; Ocampo-Torres, F.J. Dynamic analysis of a six-degree of freedom wave energy converter based on the concept of the Stewart-Gough platform. *Renew. Energy* **2020**, *146*, 1051–1061. [CrossRef]
12. Penalba, M.; Davidson, J.; Windt, C.; Ringwood, J.V. A high-fidelity wave-to-wire simulation platform for wave energy converters: Coupled numerical wave tank and power take-off models. *Appl. Energy* **2018**, *226*, 655–669. [CrossRef]
13. Liu, C.; Yang, Q.; Bao, G. Influence of hydraulic power take-off unit parameters on power capture ability of a two-raft-type wave energy converter. *Ocean Eng.* **2018**, *150*, 69–80. [CrossRef]
14. Sheng, W.; Lewis, A. Power takeoff optimization for maximizing energy conversion of wave-activated bodies. *IEEE J. Ocean. Eng.* **2016**, *41*, 529–540. [CrossRef]
15. Cargo, C.J.; Hillis, A.J.; Plummer, A.R. Optimisation and control of a hydraulic power take-off unit for a wave energy converter in irregular waves. *Proc. Inst. Mech. Eng. Part A J. Power Energy* **2014**, *228*, 462–479. [CrossRef]
16. Brito, M.; Teixeira, L.; Canelas, R.B.; Ferreira, R.M.L.; Neves, M.G. Experimental and numerical studies of dynamic behaviors of a hydraulic power take-off cylinder using spectral representation method. *J. Tribol.* **2018**, *140*. [CrossRef]
17. Brito, M.; Ferreira, R.M.L.; Teixeira, L.; Neves, M.G.; Canelas, R.B. Experimental investigation on the power capture of an oscillating wave surge converter in unidirectional waves. *Renew. Energy* **2020**, *151*, 975–992. [CrossRef]

18. Amaran, S.; Sahinidis, N.V.; Sharda, B.; Bury, S.J. Simulation optimization: A review of algorithms and applications. *Ann. Oper. Res.* **2016**, *240*, 351–380. [CrossRef]
19. Jusoh, M.A.; Daud, M.Z. Particle swarm optimisation-based optimal photovoltaic system of hourly output power dispatch using Lithium-ion batteries. *J. Mech. Eng. Sci.* **2017**, *11*, 2780–2793. [CrossRef]
20. Jusoh, M.A.; Daud, M.Z. Control strategy of a grid-connected photovoltaic with battery energy storage system for hourly power dispatch. *Int. J. Power Electron. Drive Syst.* **2017**, *8*, 1830–1840. [CrossRef]
21. Daud, M.Z.; Mohamed, A.; Hannan, M.A. An improved control method of battery energy storage system for hourly dispatch of photovoltaic power sources. *Energy Convers. Manag.* **2013**, *73*, 256–270. [CrossRef]
22. Daud, M.Z.; Mohamed, A.; Ibrahim, A.A.; Hannan, M.A. Heuristic optimization of state-of-charge feedback controller parameters for output power dispatch of hybrid photovoltaic/battery energy storage system. *Meas. J. Int. Meas. Confed.* **2014**, *49*, 15–25. [CrossRef]
23. Jusoh, M.A.; Daud, M.Z. Accurate battery model parameter identification using heuristic optimization. *Int. J. Power Electron. Drive Syst.* **2020**, *11*, 333–341. [CrossRef]
24. Giassi, M.; Göteman, M. Layout design of wave energy parks by a genetic algorithm. *Ocean Eng.* **2018**, *154*, 252–261. [CrossRef]
25. Sirigu, S.A.; Foglietta, L.; Giorgi, G.; Bonfanti, M.; Cervelli, G.; Bracco, G.; Mattiazzo, G. Techno-Economic optimisation for a wave energy converter via genetic algorithm. *J. Mar. Sci. Eng.* **2020**, *8*, 482. [CrossRef]
26. McCabe, A.P.; Aggidis, G.A.; Widden, M.B. Optimizing the shape of a surge-and-pitch wave energy collector using a genetic algorithm. *Renew. Energy* **2010**, *35*, 2767–2775. [CrossRef]
27. Calvário, M.; Gaspar, J.F.; Kamarlouei, M.; Hallak, T.S.; Guedes Soares, C. Oil-hydraulic power take-off concept for an oscillating wave surge converter. *Renew. Energy* **2020**, *159*, 1297–1309. [CrossRef]
28. Jusoh, M.A.; Ibrahim, M.Z.; Daud, M.Z.; Yusop, Z.M.; Albani, A.; Rahman, S.J.; Mohad, S. Parameters estimation of hydraulic power take-off system for wave energy conversion system using genetic algorithm. In *Proceedings of the IOP Conference Series: Earth and Environmental Science*; Institute of Physics Publishing: Bristol, UK, 2020; Volume 463, p. 12129.
29. Hansen, R.H.; Kramer, M.M.; Vidal, E.; Hansen, R.H.; Kramer, M.M.; Vidal, E. Discrete displacement hydraulic power take-off system for the wavestar wave energy converter. *Energies* **2013**, *6*, 4001–4044. [CrossRef]
30. Hansen, A.H.; Asmussen, M.F.; Bech, M.M. Model predictive control of a wave energy converter with discrete fluid power power take-off system. *Energies* **2018**, *11*, 635. [CrossRef]
31. Garcia-Rosa, P.B.; Cunha, J.P.V.S.; Lizarralde, F.; Estefen, S.F.; Costa, P.R. Efficiency optimization in a wave energy hyperbaric converter. In Proceedings of the 2009 International Conference on Clean Electrical Power, ICCEP 2009, Capri, Italy, 9–11 June 2009; pp. 68–75.
32. Estefen, S.F.; Esperança, P.D.T.; Ricarte, E.; Da Costa, P.R.; Pinheiro, M.M.; Clemente, C.H.P.; Franco, D.; Melo, E.; De Souza, J.A. Experimental and numerical studies of the wave energy hyperbaric device for electricity production. In *Proceedings of the International Conference on Offshore Mechanics and Arctic Engineering—OMAE*; American Society of Mechanical Engineers Digital Collection: New York, NY, USA, 2008; Volume 6, pp. 811–818.
33. Windt, C.; Davidson, J.; Ransley, E.J.; Greaves, D.; Jakobsen, M.; Kramer, M.; Ringwood, J.V. Validation of a CFD-based numerical wave tank model for the power production assessment of the wavestar ocean wave energy converter. *Renew. Energy* **2020**, *146*, 2499–2516. [CrossRef]
34. Ransley, E.J.; Greaves, D.M.; Raby, A.; Simmonds, D.; Jakobsen, M.M.; Kramer, M. RANS-VOF modelling of the Wavestar point absorber. *Renew. Energy* **2017**, *109*, 49–65. [CrossRef]
35. Gibraltar Project—Eco Wave Power. Available online: https://www.ecowavepower.com/gibraltar-project/ (accessed on 4 May 2019).
36. Penalba, M.; Sell, N.P.; Hillis, A.J.; Ringwood, J.V. Validating a wave-to-wire model for a wave energy converter—Part I: The hydraulic transmission system. *Energies* **2017**, *10*, 977. [CrossRef]
37. Cargo, C.J.; Plummer, A.R.; Hillis, A.J.; Schlotter, M. Determination of optimal parameters for a hydraulic power take-off unit of a wave energy converter in regular waves. *Proc. Inst. Mech. Eng. Part A J. Power Energy* **2012**, *226*, 98–111. [CrossRef]
38. Do, H.T.; Dang, T.D.; Ahn, K.K. A multi-point-absorber wave-energy converter for the stabilization of output power. *Ocean Eng.* **2018**, *161*, 337–349. [CrossRef]
39. Muzathik, A.M.; Wan Nik, W.B.; Samo, K.B.; Ibrahim, M.Z. Ocean wave measurement and wave climate prediction of Peninsular Malaysia. *J. Phys. Sci.* **2011**, *22*, 77–92.
40. Chen, Q.; Yue, X.; Geng, D.; Yan, D.; Jiang, W. Integrated characteristic curves of the constant-pressure hydraulic power take-off in wave energy conversion. *Int. J. Electr. Power Energy Syst.* **2020**, *117*, 105730. [CrossRef]
41. Jianan, X.; Tao, X. MPPT Control of Hydraulic Power Take-Off for Wave Energy Converter on Artificial Breakwater. *J. Mar. Sci. Eng.* **2019**, *8*, 304. [CrossRef]
42. Zhang, S.; Tezdogan, T.; Zhang, B.; Xu, L.; Lai, Y. Hull form optimisation in waves based on CFD technique. *Ships Offshore Struct.* **2018**, *13*, 149–164. [CrossRef]
43. Navid, A.; Khalilarya, S. Evaluation of a diesel engine optimized by non-evolutionary NLPQL and evolutionary genetic algorithms and assessing second law efficiency: Analysis in exergy loss and chemical exergy. *Appl. Therm. Eng.* **2019**, *159*. [CrossRef]

44. Navid, A.; Khalilarya, S.; Taghavifar, H. Comparing multi-objective non-evolutionary NLPQL and evolutionary genetic algorithm optimization of a DI diesel engine: DoE estimation and creating surrogate model. *Energy Convers. Manag.* **2016**, *126*, 385–399. [CrossRef]
45. Chen, Y.; Lv, L. The multi-objective optimization of combustion chamber of DI diesel engine by NLPQL algorithm. *Appl. Therm. Eng.* **2014**, *73*, 1332–1339. [CrossRef]
46. Hu, N.; Zhou, P.; Yang, J. Comparison and combination of NLPQL and MOGA algorithms for a marine medium-speed diesel engine optimisation. *Energy Convers. Manag.* **2017**, *133*, 138–152. [CrossRef]
47. Hydraulic Cylinders—Heavy Duty Roundline Welded—Series RDH | Malaysia. Available online: https://ph.parker.com/my/en/heavy-duty-hydraulic-roundline-cylinders-series-rdh (accessed on 19 January 2020).
48. Bladder Accumulator—High Pressure (EHV) | Malaysia. Available online: https://ph.parker.com/my/en/bladder-accumulator-high-pressure-ehv (accessed on 19 January 2020).
49. Bladder Accumulator—Low Pressure (EBV Series) | Malaysia. Available online: https://ph.parker.com/my/en/low-pressure-bladder-accumulator-ebv (accessed on 19 January 2020).
50. High Torque Radial Piston Motors—Series MR* | Malaysia. Available online: https://ph.parker.com/my/en/high-torque-radial-piston-motors-series-mr (accessed on 19 January 2020).